

Growth of Dust as the Initial Step Toward Planet Formation

Carsten Dominik

Universiteit van Amsterdam

Jürgen Blum

Technische Universität Braunschweig

Jeffrey N. Cuzzi

NASA Ames Research Center

Gerhard Wurm

Universität Münster

We discuss the results of laboratory measurements and theoretical models concerning the aggregation of dust in protoplanetary disks, as the initial step toward planet formation. Small particles easily stick when they collide and form aggregates with an open, often fractal structure, depending on the growth process. Larger particles are still expected to grow at collision velocities of about 1m/s. Experiments also show that, after an intermezzo of destructive velocities, high collision velocities above 10m/s on porous materials again lead to net growth of the target. Considerations of dust-gas interactions show that collision velocities for particles not too different in surface-to-mass ratio remain limited up to sizes about 1m, and growth seems to be guaranteed to reach these sizes quickly and easily. For meter sizes, coupling to nebula turbulence makes destructive processes more likely. Global aggregation models show that in a turbulent nebula, small particles are swept up too fast to be consistent with observations of disks. An extended phase may therefore exist in the nebula during which the small particle component is kept alive through collisions driven by turbulence which frustrates growth to planetesimals until conditions are more favorable for one or more reasons.

1. INTRODUCTION

The growth of dust particles by aggregation stands at the beginning of planet formation. Whether planetesimals form by incremental aggregation, or through gravitational instabilities in a dusty sublayer, particles have to grow and settle to the midplane regardless. On the most basic level, the physics of such growth is simple: Particles collide because relative velocities are induced by random and (size-dependent) systematic motions of grains and aggregates in the gaseous nebula surrounding a forming star. The details are, however, highly complex. The physical state of the disk, in particular the presence or absence of turbulent motions, set the boundary conditions. When particles collide with low velocities, they stick by mutual attractive forces, be it simple van der Waals attraction or stronger forces (molecular dipole interaction in polar ices, or grain-scale long-range forces due to charges or magnetic fields). While the lowest velocities create particle shapes governed by the motions alone, larger velocities contribute to shaping the aggregates by restructuring and destruction. The ability to internally dissipate energy is critical in the growth through intermediate pebble and boulder sizes. In this review we will concentrate on the physical properties and growth characteristics of these small and intermediate sizes, but also

make some comments on the formation of planetesimals.

Relative velocities between grains in a protoplanetary disk can be caused by a variety of processes. For the smallest grains, these are dominated by Brownian motions, that provide relative velocities in the mm/s to cm/s range for (sub)micron sized grains. Larger grains show systematic velocities in the nebula because they decouple from the gas, settle vertically, and drift radially. At 1AU in a solar nebula, these settling velocities reach m/s for cm-sized grains. Radial drift becomes important for even larger particles and reaches 10's of m/s for m-sized bodies. Finally, turbulent gas motions can induce relative motions between particles. For details see for example *Weidenschilling* (1977; 1984), *Weidenschilling and Cuzzi* (1993), *Cuzzi and Hogan* (2003).

The timescales of growth processes and the density and strength of aggregates formed by them, will depend on the structure of the aggregates. A factor of overriding importance for dust-gas interactions (and therefore for the timescales and physics of aggregation), for the stability of aggregates, and for optical properties alike is the structure of aggregates as they form through the different processes.

The interaction of particles with the nebula gas is determined primarily by their gas drag stopping time t_s which is

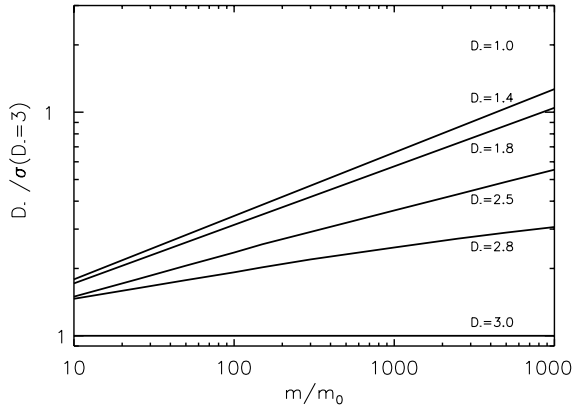


Fig. 1.— Projected area of aggregates as a function of aggregate size and fractal dimension, normalized to the cross section of a compact particle with the same mass.

given by

$$= \frac{mv}{F_{\text{fic}}} = \frac{3}{4c} \frac{m}{\rho_g \sigma} \quad (1)$$

where m is the mass of a particle, v its velocity relative to the gas, σ the average projected surface area, ρ_g is the gas density, c is the sound speed, and F_{fic} is the drag force. The second equal sign in eq.(1) holds under the assumption that particles move at sub-sonic velocities and that the mean free path of a gas molecule is large compared to the size of the particle (Epstein regime). In this case, the stopping time is proportional to the ratio of mass and cross section of the particle. For spherical non-fractal (i.e. compact or porous) particles of radius a and mass density ρ , this can be written as $\tau = a\rho / c\rho_g$. Fractal particles are characterized by the fact that the average density of a particle depends on size in a powerlaw fashion, with a power (the fractal dimension D_f) smaller than 3.

$$m(a) \propto a^{D_f} \quad (2)$$

For large aggregates, this value can in principle be measured for individual particles. For small particles, it is often more convenient to measure it using sizes and masses of a distribution of particles.

Fractal particles generally have large surface-to-mass ratios; in the limiting case of long linear chains ($D_f = 1$) of grains with radii a_0 , σ/m approaches the constant value $3\pi/(16a_0\rho)$. This value differs from the value for a single grain $3/(4a_0\rho)$ by just a factor $\pi/4$. Fig. 1 shows how the cross section of particles varies with their mass for different fractal dimensions. It shows that for aggregates made of 10000 monomers, the surface-to-mass ratio can easily differ by a factor of 10. An aggregate made from $0.1\mu\text{m}$ particles with a mass equivalent to a $10\mu\text{m}$ particle consists of 10^6 monomers and the stopping time could vary by a factor of order 100. Just how far the fractal growth of aggregates proceeds is really not yet known.

This review is organized as follows: In section 2 we cover the experiments and theory describing the basic

growth processes of dust aggregates. In section 3 we discuss particle-gas interactions and the implications for inter-particle collision velocities as well as planetesimal formation. In section 4 we describe recent advances in the modeling of dust aggregation in protoplanetary disks and observable consequences.

2. DUST AGGREGATION EXPERIMENTS AND THEORY

2.1. Interactions between individual dust grains

2.1.1 Interparticle adhesion forces. Let us assume that the dust grains are spherical in shape and that they are electrically neutral and non-magnetic. In that case, two grains with radii a_1 and a_2 will always experience a short-range attraction due to induced dielectric forces, e.g. van der Waals interaction. This attractive force results in an elastic deformation leading to a flattening of the grains in the contact region. An equilibrium is reached when the attractive force equals the elastic repulsion force. For small, hard grains with low surface forces, the equilibrium contact force is given by (Derjaguin *et al.*, 1975)

$$F_c = 4\pi\gamma R \quad (3)$$

where γ and R denote the specific surface energy of the grain material and the local radius of surface curvature, given by $R = a_2/(1 + a_2/a_1)$, respectively. Measurements of the separation force between pairs of SO_2 spheres with radii a between $0.5\mu\text{m}$ and $2.5\mu\text{m}$ (corresponding to reduced radii $R = 0.35 \dots 1.3\mu\text{m}$) confirm the validity of Eq. 3 (Heim *et al.*, 1999).

2.1.2 Interparticle rolling-friction forces. Possibly the most important parameter influencing the structure of aggregates resulting from low velocity collisions is the resistance to rolling motion. If this resistance is very strong, both aggregate compaction and internal energy dissipation in aggregates would be very difficult. Resistance to rolling first of all depends strongly on the geometry of the grains. If grains contain extended flat surfaces, contact made on such locations could not be moved by rolling - any attempt to roll them would inevitably lead to breaking the contact. In the contact between round surfaces, resistance to rolling must come from an asymmetric distribution of the stresses in the contact area. Without external forces, the net torque exerted on the grains should be zero. Dominik and Tielens (1995) showed that the pressure distribution becomes asymmetric, when the contact area is slightly shifted with respect to the axis connecting the curvature centers of the surfaces in contact. The resulting torque is

$$M = 4 \left(\frac{a_c - a_{c,t}}{a_c} \right)^{1/2} \xi \quad (4)$$

where a_c is the equilibrium contact radius, $a_{c,t}$ is the actual contact radius due to pressure in the vertical direction, and ξ is the displacement of the contact area due to

the torque. In this picture, energy dissipation, and therefore friction, occurs when the contact area suddenly readjusts after it has been displaced because of external forces acting on the grains. The friction force is proportional to the pull-off force

Heim et al. (1999) observed the reaction of a chain of dust grains using a long-distance microscope and measured the applied force with an Atomic Force Microscope (AFM). The derived rolling-friction forces between two spheres with radii of 9 m are $11 \pm 8 \cdot 10^{-5} \text{ N}$. If we recall that there are two grains involved in rolling, we get for the rolling-friction energy, defined through a displacement of an angle 2

$$E_{\text{roll}} \approx 10^{-5} \text{ J} \quad (5)$$

Recently, the rolling of particle chains has been observed under the scanning electron microscope while the contact forces were measured simultaneously (*Heim et al.*, 2005).

2.1.3 Sticking efficiency in single grain collisions. The dynamical interaction between small dust grains was derived by *Poppe et al.* (2000a) in an experiment in which single, micrometer-sized dust grains impacted smooth targets at various velocities ($\dots 0 \text{ m/s}$) under vacuum conditions. For spherical grains, a sharp transition from sticking with an efficiency of $\beta \approx 1$ to bouncing (i.e. a sticking efficiency of $\beta \approx 0$) was observed. This threshold velocity is $\approx 2 \text{ m/s}$ for 1 m and $\approx 9 \text{ m/s}$ for 2 m . It decreases with increasing grain size. The target materials were either polished quartz or atomically-smooth (surface-oxidized) silicon. Currently, no theoretical explanation is available for the threshold velocity for sticking. Earlier attempts to model the low-velocity impact behavior of spherical grains predicted much lower sticking velocities (*Chokshi et al.*, 1993). These models are based upon impact experiments with “softer” polystyrene grains (*Dahneke*, 1975). The main difference becomes visible when studying the behavior of the rebound grains in non-sticking collisions. In the experiments by *Dahneke* (1975) and also in those by *Bridges et al.* (1996) using macroscopic ice grains, the behavior of grains after a bouncing collision was a unique function of the impact velocity, with a coefficient of restitution (rebound velocity divided by impact velocity) always close to unity and increasing monotonically above the threshold velocity for sticking. For harder, still spherical, 10 m grains (*Poppe et al.*, 2000a), the average coefficient of restitution decreases considerably with increasing impact velocity. In addition to that, individual grain impacts show considerable scatter in the coefficient of restitution.

The impact behavior of irregular dust grains is more complex. Irregular grains of various sizes and compositions show an overall decrease in the sticking probability with increasing impact velocity. The transition from $\beta \approx 1$ to $\beta \approx 0$, however, is very broad so that even impacts as fast as $\approx 0 \text{ m/s}$ can lead to sticking with a moderate probability.

2.2. Dust aggregation and restructuring

2.2.1 Laboratory and microgravity aggregation experiments. In recent years, a number of laboratory and microgravity experiments have been carried out to derive the aggregation behavior of dust under conditions of young planetary systems. To be able to compare the experimental results to theoretical predictions and to allow numerical modelling of growth phases that are not accessible to experimental investigation, “ideal” systems were studied, in which the dust grains were monodisperse (i.e. all of the same size) and initially non-aggregated. Whenever the mean collision velocity between the dust grains or aggregates is much smaller than the sticking threshold (see section 2.1.3), the aggregates formed in the experiments are “fractal”, i.e. $D_f < 3$ (*Wurm and Blum*, 1998; *Blum et al.*, 1999; *Blum et al.*, 2000; *Krause and Blum*, 2004). The precise value of the fractal dimension depends on the specific aggregation process and can reach values as low as $D_f \approx 1.5$ for Brownian-motion driven aggregation (*Blum et al.*, 2000; *Krause and Blum*, 2004; *Paszun and Dominik*, 2006), $D_f \approx 1.8$ for aggregation in a turbulent gas (*Wurm and Blum*, 1998), or $D_f \approx 2.5$ for aggregation by gravitationally driven sedimentation in gas (*Blum et al.*, 1999). It is inherent to a dust aggregation process in which aggregates with low fractal dimensions are formed that the mass distribution function is rather narrow (quasi-monodisperse) at any given time. In all realistic cases, the mean aggregate mass M follows either a power law with time t , i.e. $M \propto t^\gamma$ with $\gamma < 1$ (*Krause and Blum*, 2004) or grows exponentially fast, $M \propto \exp(\delta t)$ with $\delta > 0$ (*Wurm and Blum*, 1998) which can be verified in dust-aggregation models (see Section 2.2.2).

As predicted by *Dominik and Tielens* (1995, 1996, 1997), experiments have shown that at collision velocities near the velocity threshold for sticking (of the individual dust grains), a new phenomenon occurs (*Blum and Wurm*, 2000). Whereas at low impact speeds, the aggregates’ structures are preserved in collisions (the so-called “hit-and-stick” behavior), the forming aggregates are compacted at higher velocities. In even more energetic collisions, the aggregates fragment so that no net growth is observable. The different stages of compaction and fragmentation are depicted in Fig. 2.

2.2.2 Modelling of dust aggregation. The evolution of grain morphologies and masses for a system of initially monodisperse spherical grains that are subjected to Brownian motion has been studied numerically by *Kempf et al.* (1999). The mean aggregate mass increases with time following a power law (see Section 2.2.1). The aggregates have fractal structures with a mean fractal dimension of $D_f \approx 1.8$. Analogous experiments by *Blum et al.* (2000) and *Krause and Blum* (2004), however, found that the mean fractal dimension was $D_f \approx 1.5$. Recent numerical work by *Paszun and Dominik* (2006) showed that this lower value is caused by Brownian rotation (neglected by *Kempf et al.* (1999)).

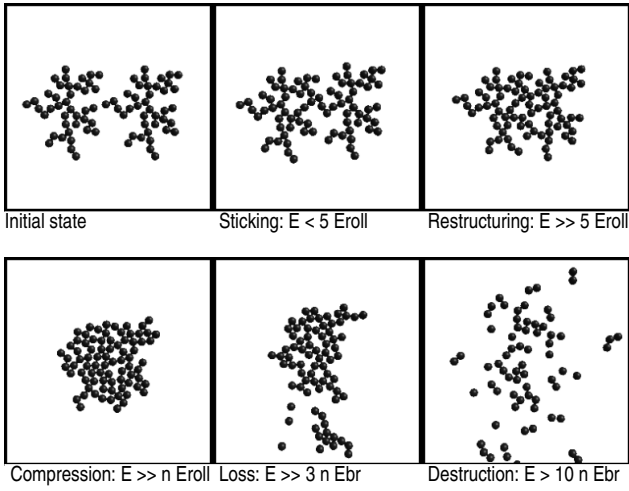


Fig. 2.— Dominating processes and associated energies in aggregate collisions, after *Dominik and Tielens* (1997) and *Wurm and Blum* (2000). E_{br} is the energy needed to break a contact, E_{roll} is the energy to roll two grains through an angle $\pi/2$ and n is the total number of contacts in the aggregates.

More chain-like dust aggregates can form if the mean free path of the colliding aggregates becomes smaller than their size, i.e. if the assumption of ballistic collisions breaks down and a random-walk must be considered for the approach of the particles. The fractal dimension of thermally aggregating dust grains is therefore dependent on gas pressure and reaches an asymptotic value of $D_f \approx 1.8$ for the low density conditions prevailing through most of the presolar nebula. Only in the innermost regions the densities are high enough to cause deviations.

The experimental work reviewed in Section 2.2.1 can be used to test the applicability of theoretical dust aggregation models. Most commonly, the mean-field approach by *Smoluchowski* (1916) is used for the description of the number density n of dust aggregates with mass m as a function of time t . Smoluchowski’s rate equation reads in the integral form

$$\frac{\partial n}{\partial t} = \frac{1}{2} \int_0^m K(m', m-m') n' n - m' \frac{dn'}{dt} - n \int_m^\infty K(m, m') n' \frac{dm'}{dt} \quad (6)$$

Here, K is the reaction kernel for aggregation of the coagulation equation 6. The first term on the rhs. of Eq. 6 describes the rate of sticking collisions between dust particles of masses m' and $m-m'$ whose combined masses are m (gain in number density for the mass m). The second term denotes a loss in the number density for the mass m due to sticking collisions between particles of mass m' and mass $m-m'$. The factor 1/2 in the first term accounts for the fact that each pair collision is counted twice in the integral. In most astrophysical applications the gas densities are so low that dust aggregates collide ballistically. In that case,

the kernel in Eq. 6 is given by

$$K(m, m') = \beta v(m, m') \sigma(m, m') \quad (7)$$

where β is the sticking probability, $v(m, m')$ is the collision velocity, and $\sigma(m, m')$ is the cross section for collisions between aggregates of masses m and m' , respectively.

A comparison between numerical predictions from Eq. 6 and experimental results on dust aggregation was given by *Wurm and Blum* (1998) who investigated dust aggregation in rarefied, turbulent gas. Good agreement for both the mass distribution functions and the temporal behavior of the mean mass was found when using a sticking probability of $\beta \approx 0.5$, a mass-independent relative velocity between the dust aggregates and the expression by *Ossenkopf* (1993) for the collision cross section of fractal dust aggregates. *Blum* (2006) showed that the mass distribution of the fractal aggregates observed by *Krause and Blum* (2004) for Brownian-motion driven aggregation can also be modelled in the transition regime between free-molecular and hydrodynamic gas flow.

Analogous to the experimental findings for the collisional behavior of fractal dust aggregates with increasing impact energy (*Blum and Wurm* (2000), see Section 2.2.1), *Dominik and Tielens* (1997) showed in numerical experiments on aggregate collisions that with increasing collision velocity the following phases can be distinguished: hit-and-stick behavior, compaction, loss of monomer grains, and complete fragmentation (see Fig. 2). They also showed that the outcome of a collision depends on the impact energy, the rolling-friction energy (see Eq. 5 in Section 2.1.2) and the energy for the breakup of single interparticle contacts (see Section 2.1.1). The model by *Dominik and Tielens* (1997) was quantitatively confirmed by the experiments of *Blum and Wurm* (2000) (see Fig. 2).

To analyze observations of protoplanetary disks and model the radiative transfer therein, the optical properties of particles are important (*McCabe et al.*, 2003; *Ueta and Meixner*, 2003; *Wolf*, 2003). Especially for particle sizes comparable to the wavelength of the radiation, the shape and morphology of a particle are of major influence for the way the particle interacts with the radiation. With respect to this, it is important to know how dust evolution changes the morphology of a particle. As seen above, in most cases dust particles are not individual monolithic solids but rather aggregates of primary dust grains. Numerous measurements and calculations have been carried out on aggregates (e.g. *Kozasa et al.*, 1992; *Henning and Stognienko*, 1996; *Wurm and Schnaiter*, 2002; *Gustafson and Kolokolova*, 1999; *Wurm et al.*, 2004a; *Min et al.*, 2005). No simple view can be given within the frame of this paper. However, it is clear that the morphology and size of the aggregates will strongly influence the optical properties.

2.2.3 Aggregation with long-range forces. Long range forces may play a role in the aggregation process, if grains are either electrically charged or magnetic. Small iron

grains may become spontaneously magnetic if they are single domain (Nuth *et al.*, 1994; Nuth and Wilkinson, 1995), typically at sizes of a few tens of nanometers. Larger grains containing ferromagnetic components can be magnetized by an impulse magnetic field generated during a lightning discharge (Túnyi *et al.*, 2003). For such magnetized grains, the collisional cross section is strongly enhanced compared to the geometrical cross section (Dominik and Nübold, 2002). Aggregates formed from magnetic grains remain strong magnetic dipoles, if the growth process keeps the grain dipoles aligned in the aggregate (Nübold and Glassmeier, 2000). Laboratory experiments show the spontaneous formation of elongated, almost linear aggregates, in particular in the presence of an external magnetic field (Nübold *et al.*, 2003). The relevance of magnetic grains to the formation of macroscopic dust aggregates is, however, unclear.

Electric charges can be introduced through tribo-electric effects in collisions, through which electrons and/or ions are exchanged between the particles (Poppe *et al.*, 2000b; Poppe and Schräpler, 2005; Desch and Cuzzi, 2000). The number of separated elementary charges in a collision between a dust particle and a solid target with impact energy can be expressed by (Poppe *et al.*, 2000b; Poppe and Schräpler, 2005)

$$N_e \approx \left(\frac{v}{v_0} \right)^{.8} \quad (8)$$

The cumulative effect of many non-sticking collisions can lead to an accumulation of charges and to the build-up of strong electrical fields at the surface of a larger aggregate. In this way, impact charging could lead to electrostatic trapping of the impinging dust grains or aggregates (Blum, 2004). Moreover, impact charging and successive charge separation can cause an electric discharge in the nebula gas. For nebula lighting (Desch and Cuzzi, 2000) a few hundred to thousand elementary charges per dust grain are required. This corresponds to impact velocities in the range $2 \dots 10 \text{ m s}^{-1}$ (Poppe and Schräpler, 2005) which seems rather high for mm particles.

Electrostatic attraction by dipole-dipole forces has been seen to be important for grains of several hundred micron radius (chondrule size) forming clumps that are centimeters to tens of centimeters across (Marshall *et al.*, 2005; Ivlev *et al.*, 2002). Spot charges distributed over the grain surfaces lead to a net dipole of the grains, with growth dynamics very similar to that of magnetic grains. Experiments in microgravity have shown spontaneous aggregation of particles in the several hundred micron size regime (Marshall and Cuzzi, 2001; Marshall *et al.*, 2005; Love and Pettit, 2004). The aggregates show greatly enhanced stability, consistent with cohesive forces increased by factors of 10 compared to the normal van der Waals interaction. Based on the experiments, for weakly charged dust grains, the electrostatic interaction energy at contact for the charge-dipole interaction is in most cases larger than that for the charge-charge

interaction. For heavily-charged particles, the mean mass of the system does not grow faster than linearly with time, i.e. even slower than in the non-charged case for Brownian motion (Ivlev *et al.*, 2002; Konopka *et al.*, 2005).

2.3. Growth and compaction of large dust aggregates

2.3.1 Physical properties of macroscopic dust aggregates. Macroscopic dust aggregates can be created in the laboratory by a process termed random ballistic deposition (RBD, Blum and Schräpler, 2004). In its idealized form, RBD uses individual, spherical and monodisperse grains which are deposited randomly but unidirectionally on a semi-infinite target aggregate. The volume filling factor ϕ of these aggregates, defined as the fraction of the volume filled by dust grains, is identical to ballistic particle-cluster aggregation which occurs when a bimodal size distribution of particles (aggregates of one size and individual dust grains) is present and when the aggregation rates between the large aggregates and the small particles exceed those between all other combinations of particle sizes. When using idealized experimental parameters, i.e. monodisperse spherical grains with $7 \text{ }\mu\text{m}$ radius, Blum and Schräpler (2004) measured a mean volume filling factor for their macroscopic (cm-sized) RBD dust aggregates of $\phi \approx 0.5$, in full agreement with numerical predictions (Watson *et al.* 1997). Relaxing the idealized grain morphology resulted in a decrease of the volume filling factor to values of $\phi \approx 0.3$ for quasi-monodisperse, irregular diamond grains and $\phi \approx 0.1$ for polydisperse, irregular grains (Blum, 2004).

Static uniaxial compression experiments with the macroscopic RBD dust aggregates consisting of monodisperse spherical grains (Blum and Schräpler, 2004) showed that the volume filling factor remains constant as long as the stress on the sample is below $\sim 10^4 \text{ N m}^{-2}$. For higher stresses, the volume filling factor monotonically increases from $\phi \approx 0.5$ to $\phi \approx 0.8$. Above $\sim 10^5 \text{ N m}^{-2}$, the volume filling factor remains constant at $\phi \approx 0.8$. Thus, the compressive strength of the uncompressed sample is $\Sigma \approx 10^4 \text{ N m}^{-2}$. These values differ from those derived with the models of Greenberg *et al.* (1995) and Sirono and Greenberg (2000) by a factor of a few. The compressive strengths of the macroscopic dust aggregates consisting of irregular and polydisperse grains was slightly lower at $\Sigma \sim 2 \times 10^4 \text{ N m}^{-2}$. The maximum compression of these bodies was reached for stresses above $\sim 10^6 \text{ N m}^{-2}$ and resulted in volume filling factors as low as $\phi \approx 0.2$ (Blum, 2004). As a maximum compressive stress of $\sim 10^5 \dots 10^6 \text{ N m}^{-2}$ corresponds to impact velocities of $\sim 100 \dots 1000 \text{ m s}^{-1}$ which are typical for meter-sized protoplanetary dust aggregates, we expect a maximum volume filling factor for these bodies in the solar nebula of $\phi \approx 0.2 \dots 0.5$. Blum and Schräpler (2004) also measured the tensile strength of their aggregates and found for slightly compressed samples ($\phi \approx 0.2$) $T \approx 10^4 \text{ N m}^{-2}$. Depending on the grain shape and the size distribution, the tensile strength decreased to

values of $T \sim 2 \text{ N m}$ for the uncompressed case (Blum, 2004).

Sirono (2004) used the above continuum properties of macroscopic dust aggregates, i.e. compressive strength and tensile strength, to model the collisions between protoplanetary dust aggregates. For sticking to occur in an aggregate-aggregate collision, Sirono (2004) found that the impact velocity must follow the relation

$$v < \sqrt{\frac{d \Sigma \phi}{\rho \phi}} \quad (9)$$

where ϕ is the mass density of the aggregate and ρ denotes the mass density of the grain material. Moreover, the conditions $\Sigma \phi < Y \phi$ and $\Sigma \phi < T \phi$ must be fulfilled. For the shear strength, Sirono (2004) applies $Y \phi = \sqrt{2 \Sigma \phi T \phi}$. A low compressive strength of the colliding aggregates favors compaction and, thus, damage restoration which can otherwise lead to a break-up of the aggregates. In addition, a large tensile strength also prevents the aggregates from being disrupted in the collision.

Blum and Schr ppler (2004) found an approximate relation between compressive strength and volume filling factor

$$\Sigma \phi = \Sigma \phi \phi^8 \quad (10)$$

which is valid in the range $\phi \leq \phi \leq 2$. Such a scaling law was also found for other types of macroscopic aggregates, e.g. for jammed toner particles in fluidized bed experiments (Valverde et al., 2004). For the aggregates consisting of monodisperse spheres, the scaling factor Σ can be determined to be $\Sigma = 2.9 \cdot 10^4 \text{ N m}^{-1}$. If we apply Eq. 10 to Eq. 9, we get, with $\phi = \phi$ and $\rho = 2000 \text{ kg m}^{-3}$, for the impact velocity of low-density dust aggregates

$$v < \sqrt{\frac{8 \Sigma}{\phi \phi}} \approx \phi \phi \text{ m s} \quad (11)$$

Although the function in Eq. 11 goes to infinity for $\phi \rightarrow \phi$, for all practical purposes the characteristic velocity is strongly restricted. For volume filling factors $\phi \geq 1$ we get $v < 22 \text{ m s}$. Thus, following the SPH simulations by Sirono (2004), we expect aggregate sticking in collisions for impact velocities $v \lesssim 2 \text{ m s}$.

2.3.2 Low-velocity collisions between macroscopic dust aggregates. Let us now consider recent results in the field of high-porosity aggregate collisions. Langkowski and Blum (unpublished data) performed microgravity collision experiments between 0.1-1 mm-sized (projectile) RBD aggregates and 2.5 cm-sized (target) RBD aggregates. Both aggregates consisted of monodisperse spherical grains with radii of $r = 7 \text{ }\mu\text{m}$. In addition to that, impact experiments with high-porosity aggregates consisting of irregular and/or polydisperse grains were performed. The parameter space of the impact experiments by Langkowski and Blum encompassed collision velocities in the range $v < 1 \text{ m s}$

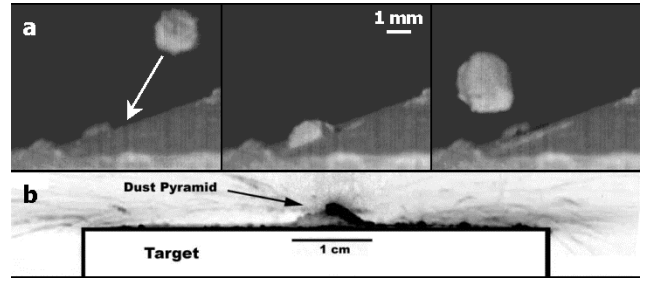


Fig. 3.— (a) Non-sticking ($v=1.8 \text{ m/s}$) oblique impact between high-porosity dust aggregates (Langkowski and Blum, unpublished data). The three images show, from left to right, the approaching projectile aggregate before, during, and after impact. The arrow in the left image denotes the impact direction of the projectile aggregate. The experiment was performed under microgravity conditions. It is clearly visible that the rebounding aggregate (right image) is more massive than before the collision. (b) Result of a high-velocity normal impact ($v = 23.7 \text{ m/s}$) between compacted aggregates (Wurm et al., 2005). About half of the projectile mass sticks to the target after the impact and is visible by its pyramidal structure on the flat target. Mind the different size scales in (a) and (b).

$v < 1 \text{ m s}$ and projectile masses of $10^{-9} \text{ kg} \leq m \leq 1 \text{ kg}$ for all possible impact parameters (i.e. from normal to tangential impact). Surprisingly, through most of the parameter space, the collisions did lead to sticking. The experiments with aggregates consisting of monodisperse spherical grains show, however, a steep decrease in sticking probability from $\beta = 1$ to $\beta \approx 0$ if the tangential component of the impact energy exceeds $\sim 1 \text{ J}$ (see the example of a non-sticking impact in Fig. 3a). Other materials also show the tendency towards lower sticking probabilities with increasing tangential impact energies. As these aggregates are “softer”, the decline in sticking probability in the investigated parameter space is not complete. When the projectile aggregates did not stick to the target aggregate, considerable mass transfer from the target to the projectile aggregate takes place during the impact (Langkowski and Blum, unpublished data). Typically, the mass of the projectile aggregate was doubled after a non-sticking collision (see Fig. 3a).

The occurrence of sticking in aggregate-aggregate collisions at velocities $v \gtrsim 1 \text{ m s}$ is clearly in disagreement with the prediction by Sirono (2004) (see Eq. 9). In addition, the evaluation of the experimental data shows that the condition for sticking, $\Sigma \phi < Y \phi$, seems not to be fulfilled for high-porosity dust aggregates. This means that the continuum aggregate model by Sirono (2004) is still not precise enough to fully describe the collision and sticking behavior of macroscopic dust aggregates.

2.3.3 High-velocity collisions between macroscopic dust aggregates. The experiments described above indicate that at velocities above approximately 1 m/s, collisions turn from sticking to bouncing, at least for oblique impacts. At higher velocities one would naively expect that bouncing

and eventually erosion will continue to dominate, and this is also observed in a number of different experiments (Colwell, 2003; Bridges *et al.* 1996, Kouchi *et al.*, 2002; Blum and Münch, 1993; Blum and Wurm, 2000).

Growth models which assume sticking at velocities \gg m s are therefore often considered to be impossible (e.g. Youdin, 2004). As velocities m s clearly occur for particles that have exceeded m-size, this is a fundamental problem for the formation of planetesimals.

However, recent experiments (Wurm *et al.*, 2005) have studied impacts of mm-sized compact dust aggregates onto cm-sized compact aggregate targets at impact velocities between 6 and 25 m s. Compact aggregates can be the result of previous sticking or non-sticking collisions (see Sections 2.3.1 and 2.3.2). Both projectile and target consisted of m-sized dust particles. In agreement with the usual findings at lower impact velocities around a few m s, the projectiles just rebound, slightly fracture or even remove some parts of the target. However, as the velocity increases above a threshold of 13 m s, about half of the mass of the projectile rigidly sticks to the target after the collision while essentially no mass is removed from the target (see Fig. 3b). Obviously, higher collision velocities can be favorable for growth, probably by destroying the internal structure of the porous material and dissipating energy in this way.

Only about half of the impactor contributes to the growth of the target in the experiments. The other half is ejected in the form of small fragments, with the important implication that these collisions both lead to net growth of the target and return small particles to the disk. This keeps dust abundant in the disk over a long time. For the specific experiments by Wurm *et al.* (2005), the fragments were evenly distributed in size up to 0.5 mm. In a certain sense, the disk might thus quickly turn into a “debris disk” already at early times. We will get back to this point in section 4.4.

3. PARTICLE-GAS INTERACTION

Above we have seen that small solid particles grow rapidly into aggregates of quite substantial sizes, while retaining their fractal nature (in the early growth stage) or a moderate to high porosity (for later growth stages). From the properties of primitive meteorites, we have a somewhat different picture of nebula particulates - most of the solids (chondrules, CAIs, metal grains, etc) were individually compacted as the result of unknown melting processes, and were highly size-sorted. Even the porosity of what seem to be fine-grained accretion rims on chondrules is 25% or less (Scott *et al.*, 1996; Cuzzi, 2004; Wasson *et al.*, 2005). Because age-dating of chondrules and chondrites implies a delay of a Myr or more after formation of the first solids, it seems possible that, in the asteroid formation region at least, widespread accretion to parent body sizes did not occur until after the mystery melting events began which formed the chondrules.

It may be that conditions differed between the inner and outer solar system. Chondrule formation might not have

occurred at all in the outer solar system where comet nuclei formed, so some evidence of the fractal aggregate growth stage may remain in the granular structure of comet nuclei. New results from Deep Impact imply that comet Tempel 1 has a porosity of 60-80% (A’Hearn *et al.*, 2005)! This value is in agreement with similar porosities found in several other comets (Davidsson, 2006). Even in the terrestrial planet/asteroid belt region, there is little reason to doubt that growth of aggregates started well before the chondrule formation era, and continued into and (probably) throughout it. Perhaps, after chondrules formed, previously ineffective growth processes might have dominated (sections 3.2 and 3.3).

3.1. Radial and vertical evolution of solids

3.1.1 Evolution prior to formation of a dense midplane layer. The nebula gas (but not the particles) experiences radial pressure gradients because of changing gas density and temperature. These pressure gradients act as small modifications to the central gravity from the star that dominates orbital motion, so that the gas and particles orbit at different speeds and a gas drag force exists between them which constantly changes their orbital energy and angular momentum. Because the overall nebula pressure gradient force is outward, it counteracts a small amount of the inward gravitational force and the gas generally orbits more slowly than the particles, so the particles experience a headwind which saps their orbital energy, and the dominant particle drift is inward. Early work on gas-drag related drift was by Whipple (1972), Adachi *et al.* (1976), and Weidenschilling (1977). Analytical solutions for how particles interact with a non-turbulent nebula having a typically outward pressure gradient were developed by Nakagawa *et al.* (1986). For instance, the ratio of the pressure gradient force to the dominant central gravity is $\eta \sim 2 \times 10^{-5}$, leading to a net velocity difference between the gas and particles orbiting at Keplerian velocity V_K of ηV_K (see, e.g. Nakagawa *et al.* 1986). However, if local radial maxima in gas pressure exist, particles will drift towards their centers from both sides, possibly leading to radial bands of enhancement of solids (see section 3.4.1).

Small particles generally drift slowly inwards, at perhaps a few cm/s; even this slow inexorable drift has generated some concern over the years, as to how CAIs (early, high-temperature condensates) can survive over the apparent 1-3 Myr period between their creation and the time they were incorporated into chondrite meteorite parent bodies. This concern, however, neglected the role of turbulent diffusion (see Section 3.1.2). Particles of meter size drift inwards very rapidly - 1 AU/century. It has often been assumed that these particles were “lost into the sun”, but more realistically, their inward drift first brings them into regions warm enough to evaporate their primary constituents, which then become entrained in the more slowly evolving gas and increase in relative abundance as inward migration of solids supplies material faster than it can be removed. Early mod-

els describing significant global redistribution of solids relative to the nebula gas by radial drift were presented by *Morfill and Völk* (1984) and *Stepinski and Valageas* (1996, 1997); these models either ignored midplane settling or made simplifying approximations regarding it, and did not emphasize the potential for enhancing material in the vapor phase. Indeed, however, because of the large mass fluxes involved, this “evaporation front” effect can alter the nebula composition and chemistry significantly (*Cuzzi et al.*, 2003; *Cuzzi and Zahnle*, 2004; *Yurimoto and Kuramoto*, 2004; *Krot et al.*, 2005; *Ciesla and Cuzzi*, 2005); see also *Cyr et al.* (1999) for a discussion; however, the results of this paper are inconsistent with similar work by *Supulver and Lin* (2000) and *Ciesla and Cuzzi* (2005). This stage can occur very early in nebula history, long before formation of objects large enough to be meteorite parent bodies.

3.1.2 The role of turbulence. The presence or absence of gas turbulence plays a critical role in the evolution of nebula solids. There is currently no widespread agreement on just how the nebula gas may be maintained in a turbulent state across all regions of interest, if indeed it is (*Stone et al.*, 2000, *Cuzzi and Weidenschilling*, 2005). Therefore we discuss both turbulent and non-turbulent situations. For simplicity we will treat turbulent diffusivity \mathcal{D} as equal to turbulent viscosity $\nu_T \propto H$, where H is the nebula sound speed and vertical scale height, and $\alpha \ll 1$ is a non-dimensional scaling parameter. Evolutionary timescales of observed protoplanetary nebulae suggest that $10^{-5} < \alpha < 1$ in some global sense. The largest eddies in turbulence have scale sizes $H\sqrt{\alpha}$ and velocities $u_b \sim \sqrt{\alpha}$ (*Shakura et al.*, 1978; *Cuzzi et al.*, 2001).

Particles respond to forcing by eddies of different frequency and velocity as described by *Völk et al.* (1980) and *Markiewicz et al.* (1991), determining their relative velocities with respect to the gas and to each other. The diffusive properties of MRI turbulence, at least, seem not to differ in any significant way from the standard homogeneous, isotropic models in this regard (*Johansen and Klahr*, 2005). Analytical solutions for resulting particle velocities in these regimes were derived by *Cuzzi and Hogan* (2003). These are discussed in more detail below and by *Cuzzi and Weidenschilling* (2005).

Vertical turbulent diffusion at intensity α maintains particles of stopping time τ in a layer of thickness $h \sim H \frac{\tau}{\Omega}$ (*Dubrulle et al.*, 1995; *Cuzzi et al.*, 1996), or a solid density enhancement $H \frac{h}{\tau} \sim \frac{\Omega}{\alpha}$ above the average value. For particles of 10 cm size and smaller and $\alpha > \alpha_m \sim 10^{-6}$ cm (*Cuzzi and Weidenschilling*, 2005), the resulting layer is much too large and dilute for collective particle effects to dominate gas motions, so radial drift and diffusion continue unabated. Outward radial diffusion relieves the long-standing worry about “loss into the sun” of small particles, such as CAIs, which are too small to sediment into any sort of midplane layer unless turbulence is vanishingly small ($\alpha \ll \alpha_m$), and allows some fraction of them to survive over 1 to several Myrs after their

formation as indicated by meteoritic observations (*Cuzzi et al.*, 2003). A similar effect might help explain the presence of crystalline silicates in comets (*Bockelée-Morvan*, 2002; *Gail*, 2004).

3.1.3 Dense midplane layers. When particles *are* able to settle to the midplane, the particle density gets large enough to dominate the motions of the local gas. This is the regime of *collective effects*; that is, the behavior of a particle depends indirectly on how all other local particles combined affect the gas in which they move. In regions where collective effects are important, the mass-dominant particles can drive the entrained gas to orbit at nearly Keplerian velocities (if they are sufficiently well coupled to the gas), and thus the headwind the gas can exert upon the particles diminishes from ηV_K (section 3.1.1). This causes the headwind-driven radial drift and all other differential particle velocities caused by gas drag to diminish as well.

The particle mass loading ρ_p cannot increase without limit as particles settle, even if the global turbulence vanishes, and the density of settled particle layers is somewhat self-limiting. The relative velocity solutions of *Nakagawa et al.* (1986) apply in particle-laden regimes once ρ_p is known, but do not provide for a fully self-consistent determination of ρ_p in the above sense; this was addressed by *Weidenschilling* (1980) and subsequently *Cuzzi et al.* (1993), *Champney et al.* (1995), and *Dobrovolskis et al.* (1999). The latter numerical models are similar in spirit to the simple analytical solutions of *Dubrulle et al.* (1995) mentioned earlier, but treat large particle, high mass loading regimes in globally nonturbulent nebulae which the analytic solutions cannot address. Basically, as the midplane particle density increases, local, entrained gas is accelerated to near-Keplerian velocities by drag forces from the particles. Well above the dense midplane, the gas still orbits at its pressure-supported, sub-Keplerian rate. Thus there is a vertical shear gradient in the orbital velocity of the gas, and the velocity shear creates turbulence which stirs the particles. This is sometimes called “self-generated turbulence”. Ultimately a steady-state condition arises where the particle layer thickness reaches an equilibrium between downward settling and upward diffusion. This effect acts to block a number of gravitational instability mechanisms in the midplane (section 3.3.2).

3.2. Relative velocities and growth in turbulent and nonturbulent nebulae

In both turbulent and nonturbulent regimes, particle relative velocities drive growth to larger sizes. Below we show that relative velocities in both turbulent and nonturbulent regimes are probably small enough for accretion and growth to be commonplace and rapid, at least until particles reach meter size or so. We only present results here for particles up to a meter or so in size, because the expression for gas drag takes on a different form at larger sizes. As particles grow, their mass per unit area increases so they are less easily influenced by the gas, and “decouple” from it. Their

overall drift velocities and relative velocities all diminish roughly in a linear fashion with particle radius larger than a meter or so (Cuzzi and Weidenschilling, 2005).

We use particle velocities relative to the gas as derived by Nakagawa *et al.* (1986) for a range of local particle mass density relative to the gas density (their equations 2.11, 2.12, and 2.21) to derive particle velocities relative to each other in the same environment; all relative velocities scale with ηV_K .

For simplicity we will assume particles which differ by a factor of three in radius; Weidenschilling (1997) finds mass accretion to be dominated by size spreads on this order; the results are insensitive to this factor. Relative velocities for particles of radii a and $a/3$, in the absence of turbulence and due only to differential, pressure-gradient-driven gas drag, are plotted in the top two panels of Fig. 4. In the top panel we show cases where collective effects are negligible (particle density $\rho_p \ll$ gas density ρ_g). Differential vertical settling (shown at different heights z above the midplane, as normalized by the gas vertical scale height H) dominates relative velocities and particle growth high above the midplane $z/H > 1$, and radial relative velocities dominate at lower elevations. Except for the largest particles, relative velocities for particles with this size difference are much less than ηV_K ; particles closer in mass would have even smaller relative velocities.

Moreover, in a dense midplane layer, when collective effects dominate (section 3.1.3), all these relative velocities are reduced considerably from the values shown. In the second panel we show radial and azimuthal relative velocities for several values of ρ_p/ρ_g . When the particle density exceeds the gas density, collective effects reduce the headwind, and all relative velocities diminish.

Relative velocities in turbulence of several different intensities, as constrained by the nebula α (again for particles of radii a and $a/3$), are shown in the two bottom panels. In the second panel from the bottom, relative velocities are calculated as the difference of their velocities relative to the turbulent gas, neglecting systematic drifts and using analytical solutions derived by Cuzzi and Hogan (2003; their equation 20) to the formalism of Völk *et al.* (1980). Here, the relative velocities are forced by turbulent eddies with a range of size scales, having eddy turnover times ranging from the orbit period (for the large eddies) to much smaller values (for the smaller eddies), and scale with α .

In the bottom panel we sum the various relative velocities in quadrature to get an idea of total relative velocities in a turbulent nebula in which particles are also evolving by systematic gas-pressure-gradient driven drift. This primarily increases the relative velocities of the larger particles in the lower α cases.

Overall, keeping in mind the critical velocities for sticking discussed in section 2 (\sim m/s), and that particle surfaces are surely crushy and dissipative, one sees that for particles up to a meter or so, growth by sticking is plausible even in turbulent nebulae for a wide range of α . Crushy aggregates will grow by accumulating smaller crushy aggre-

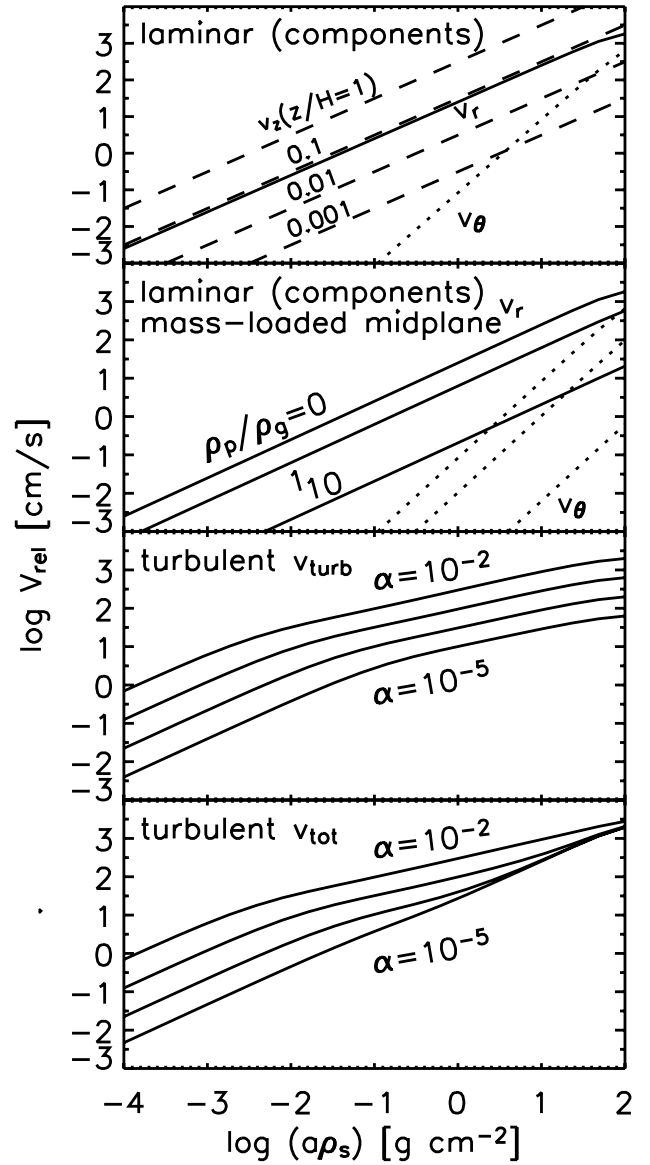


Fig. 4.— Relative velocities between particles of radii a and $a/3$, in nebulae which are non-turbulent (top two panels) or turbulent (bottom two panels), for a minimum mass solar nebula at 2.5AU. In the top panel, the particle density ρ_p is assumed to be much smaller than the gas density ρ_g : $\rho_p/\rho_g \ll 1$. Shown are the radial (solid line) and azimuthal (dotted line) components of the relative velocities. The dashed curves show the vertical relative velocities, which depend on height above the midplane and are shown for different values of z/H . For nonturbulent cases, particles settle into dense midplane layers (section 3.1.3), so a more realistic situation would be $\rho_p/\rho_g \gtrsim 1$ or even $\gg 1$ (Cuzzi *et al.*, 1993); thus in the second panel we show relative radial and angular velocities for three different values of $\rho_p/\rho_g = 0, 1, \text{ and } 10$. For these high mass loadings, z/H must be small, so the vertical velocities are smaller than the radial velocities. In the third panel we show relative velocities for the same particle size difference due only to turbulence, for several values of α . In the bottom panel, we show the quadrature sum of turbulent and non-turbulent velocities, assuming $z/H = 0.01$.

gates as described in earlier sections (eg. *Weidenschilling*, 1997, for the laminar case). After this burst of initial growth to roughly meter size, however, the evolution of solids is very sensitive to the presence or absence of global nebula turbulence, as described in sections 3.3-3.4 below. Meter-sized particles inevitably couple to the largest eddies, with $v_{\text{b}} \sim 10$ m/s, and would destroy each other if they were to collide. We refer to this as the fragmentation limit. However, if particles can somehow grow their way past 10 meters in size, their survival becomes more assured because all relative velocities, such as shown in Fig. 4, decrease linearly with r for values larger than shown in the plot due to the linear decrease of the area/mass ratio.

3.2.1 Another role of gas in growth beyond the fragmentation limit. The role of gas in protoplanetary disks is not restricted to generate relative velocities between two bodies which then collide. The gas also plays an important role *during* individual collisions. A large body which moves through the disk faces a headwind and collisions with smaller aggregates take place at its front (headwind) side. Fragments are thus ejected against the wind and can be driven back to the surface by the gas flow.

For small bodies the gas flow can be regarded as free molecular flow. Thus streamlines end on the target surface and the gas drag is always towards the surface. Whether a fragment returns to the surface depends on its gas-particle coupling time (i.e. size and density) and on the ejection speed and angle. Whether reaccretion of enough fragments for net growth occurs, eventually depends on the distribution of ejecta parameters, gas density, and target size. It was shown by *Wurm et al.* (2001) that growth of a larger body due to impact of dust aggregates entrained in a head wind is possible for collision velocities above 12m/s. At 1 AU a 30-cm body in a disk model according to *Weidenschilling and Cuzzi* (1993) can grow in a collision with small dust aggregates even if the initial collision is rather destructive.

Sekiya and Takeda (2003) and *Künzli and Benz* (2003) showed that the mechanism of aerodynamic reaccretion might be restricted to a maximum size due to a change in the flow regime from molecular to hydrodynamic. Fragments are then transported around the target rather than back to it. *Wurm et al.* (2004b) argue that very porous targets would allow some flow going through the body, which would still allow aerodynamic reaccretion, but this strongly depends on the morphology of the body (*Sekiya and Takeda*, 2005). As the gas density decreases outwards in protoplanetary disks, the maximum size for aerodynamic reaccretion increases. However, the minimum size also increases and the mechanism is only important for objects which have already grown beyond the fragmentation limit in some other way - e.g. by immediate sticking of parts of larger particles as discussed above (*Wurm et al.*, 2005).

3.3. Planetesimal formation in a midplane layer

3.3.1 Incremental growth. Based on relative velocity arguments such as given above, *Weidenschilling* (1988, 1997)

and *Dullemond and Dominik* (2004, 2005) find that growth to meter size is rapid (100-1000 yr at 1 AU; $6-7 \times 10^4$ yrs at 30 AU) whether the nebula is turbulent or not. Such large particles settle towards the midplane within an orbit period or so. However, in turbulence, even meter-sized particles are dispersed sufficiently that the midplane density remains low, and growth remains slow. A combination of rapid radial drift, generally erosive, high-velocity impacts with smaller particles, and occasional destructive collisions with other meter-sized particles frustrates growth beyond meter-size or so under these conditions.

In *nonturbulent* nebulae, even smaller particles can settle into fairly thin midplane layers and the total particle densities can easily become large enough for collective effects to drive the entrained midplane gas to Keplerian, diminishing both headwind-induced radial drift and relative velocities. In this situation, meter-sized particles quickly grow their way out of their troublesome tendency to drift radially (*Cuzzi et al.*, 1993); planetesimal-sized objects form in only 10^3 years at 1 AU (*Weidenschilling*, 2000), and a few times 10^4 years at 30 AU (*Weidenschilling*, 1997). However, such robust growth may, in fact, be too rapid to match observations of several kinds (see section 4.4 and chapters by *Dullemond et al.* and *Natta et al.*)

3.3.2 Particle layer instabilities. While to some workers the simplicity of “incremental growth” by sticking in the dense midplane layer of a nonturbulent nebula is appealing, past uncertainty in sticking properties has led others to pursue instability mechanisms for particle growth which are insensitive to these uncertainties. Nearly all instability mechanisms discussed to date (*Safronov*, 1969, 1991; *Goldreich and Ward*, 1973; *Ward*, 1976, 2000; *Sekiya*, 1983, 1998; *Goodman and Pindor*, 2000; *Youdin and Shu*, 2002) occur *only* in nebulae where turbulence is essentially absent, and particle relative velocities are already very low. Just how low the global turbulence must be depends on the particle size involved, and the nebula α (sections 3.1.1 and 3.1.3).

Classical treatments (the best known is *Goldreich and Ward*, 1973) assume that gas pressure plays no role in gravitational instability, being replaced by an effective pressure due to particle random velocities (below we note this is not the case). Particle random velocities act to puff up a layer and reduce its density below the critical value, which is always on the order of the so-called Roche density $\rho^* \sim \frac{3}{4\pi} \frac{M_{\odot}}{r^3}$ where r is the distance to the central star; different workers give constraints which differ by factors of order unity (cf. *Goldreich and Ward*, 1973, *Weidenschilling*, 1980; *Safronov*, 1991; *Cuzzi et al.*, 1993). These criteria can be traced back through *Goldreich and Ward* (1973) to *Goldreich and Lynden-Bell* (1965), *Toomre* (1964), *Chandrasekhar* (1961) and *Jeans* (1928), and in parallel through *Safronov* (1960), *Bel and Schatzman* (1958), and *Gurevitch and Lebedinsky* (1950). Substituting typical values one derives a formal, nominal requirement that the local particle mass density must exceed about 10^{-7} g cm⁻³ at 2 AU from a solar mass star even for *marginal* gravitational instability

- temporary gravitational clumping of small amplitude - to occur. This is about $\sim 10^3$ times larger than the gas density of typical minimum mass nebulae, requiring enhancement of the solids by a factor of about $\sim 10^3$ for a typical average solids-to-gas ratio. From section 3.1.2 we thus require the particle layer to have a thickness $< 5H$, which in turn places constraints on the particle random velocities Ω and on the global value of α .

Even assuming global turbulence to vanish, *Weidenschilling* (1980, 1984) noted that turbulence stirred by the very dense particle layer itself will puff it up to thicknesses that precluded even this marginal gravitational instability. This is because turbulent eddies induced by the vertical velocity profile of the gas (section 3.1.3) excite random velocities in the particles, diffusing the layer and preventing it from settling into a sufficiently dense state. Detailed two-phase fluid models by *Cuzzi et al.* (1993), *Champney et al.* (1995), and *Dobrovolskis et al.* (1999) confirmed this behavior.

It is sometimes assumed that ongoing, but slow, particle growth to larger particles, with lower relative velocities and thus thinner layers (section 3.2), can lead to $\tau_p \sim \tau_{\text{collapse}}$ and gravitational instability can then occur. However, merely achieving the formal requirement for marginal gravitational instability does not inevitably lead to planetesimals. For particles which are large enough to settle into suitably dense layers for *marginal* instability under self-generated turbulence (*Weidenschilling*, 1980; *Cuzzi et al.*, 1993) random velocities are not damped on a collapse timescale, so incipient instabilities merely “bounce” and tidally diverge. This is like the behavior seen in Saturn’s A ring, much of which is gravitationally unstable by these same criteria (*Salo*, 1992; *Karjalainen and Salo*, 2004). Direct collapse to planetesimals is much harder to achieve, requiring much lower relative velocities, and is unlikely to have occurred this way (*Cuzzi et al.* 1994, *Weidenschilling*, 1995; *Cuzzi and Weidenschilling*, 2005). Recent results by *Tanga et al.* (2004) assume an artificial damping by gas drag and find gravitationally bound clumps form which, while not collapsing directly to planetesimals, retain their identity for extended periods, perhaps allowing for slow shrinkage; this is worth further numerical modeling with more realistic damping physics, but still presumes a globally laminar nebula.

For very small particles ($< 1\text{mm}$; the highly relevant chondrule size), a different type of instability comes into play because the particles are firmly trapped to the gas by their short stopping times, and the combined system forms a single “one-phase” fluid which is stabilized against producing turbulence by its vertical density gradient (*Sekiya*, 1998; *Youdin and Shu*, 2002; *Youdin and Chiang*, 2004; *Garaud and Lin*, 2004). Even for midplane layers of such small particles to *approach* a suitable density for this to occur requires nebula turbulence to drop to what may be implausibly low values ($\alpha < 10^{-8}$ to 10^{-9}). Moreover, such one-phase layers, with particle stopping times much less than the dynamical collapse time G_p , cannot become “unstable” and collapse on the dynamical timescale as nor-

mally envisioned, because of *gas* pressure support, which is usually ignored (*Sekiya*, 1983; *Safronov*, 1991). *Sekiya* (1983) finds that particle densities must exceed $\sim 10^3$ for such particles to undergo instability and actually collapse. While especially difficult on one-phase instabilities by definition, this obstacle should be considered for any particle with stopping time much shorter than the dynamical collapse time - that is, pretty much anything smaller than a meter for $\tau_p \sim \tau_{\text{collapse}}$.

A slower “sedimentation” from axisymmetric rings (or even localized blobs of high density, which might form through fragmentation of such dense, differentially rotating rings), has also been proposed to occur under conditions normally ascribed to marginal gravitational instability (*Sekiya*, 1983; *Safronov*, 1991; *Ward*, 2000), but this effect has only been modeled under nonturbulent conditions where, as mentioned above, growth can be quite fast by sticking alone. In a turbulent nebula, diffusion (or other complications discussed below, such as large vortices, spiral density waves, etc) might preclude formation of all but the broadest-scale “rings” of this sort, which have radial scales comparable to H and grow only on extremely long timescales.

3.4. Planetesimal formation in turbulence

A case can be made that astronomical, asteroidal, and meteoritic observations require planetesimal growth to stall at sizes much smaller than several km, for something like a million years (*Dullemond and Dominik*, 2005; *Cuzzi and Weidenschilling*, 2005; *Cuzzi et al.*, 2005). This is perhaps most easily explained by the presence of ubiquitous weak turbulence ($\alpha > 10^{-3}$). Once having grown to meter-size, particles couple to the largest, most energetic turbulent eddies, leading to mutual collisions at relative velocities on the order of $v_b \sim \bar{\alpha} \sim 10\text{ m/s}$, which are probably disruptive, stalling incremental growth by sticking at around a meter in size. Astrophysical observations supporting this inference are discussed in the next section. In principle, planetesimal formation could merely await cessation of nebula turbulence and then happen all at once; pros and cons of this simple concept are discussed by *Cuzzi and Weidenschilling* (2005). The main difficulty with this concept is the very robust nature of growth in dense midplane layers of nonturbulent nebulae, compared to the very extended duration of $\sim 10^6$ years which apparently characterized meteorite parent body formation (chapter by *Wadhwa et al.*). Furthermore, if turbulence merely ceased at the appropriate time for parent body formation to begin, particles of all sizes would settle and accrete together, leaving unexplained the very well characterized chondrite size distributions we observe. Alternately, several suggestions have been advanced as to how the meter-sized barrier might be overcome even in ongoing turbulence, as described below.

3.4.1 Concentration of boulders in large nebula gas structures. The speedy inward radial drift of meter-sized particles in nebulae where settling is precluded by turbulence

might be slowed if they can be, even temporarily, trapped by one of several possible fluid dynamical effects. It has been proposed that such trapping concentrates them and leads to planetesimal growth as well.

Large nebula gas dynamical structures such as systematically rotating vortices (not true turbulent eddies) have the property of concentrating large boulders near their centers (*Barge and Sommeria*, 1995; *Tanga et al.*, 1996; *Bracco et al.*, 1998; *Godon and Livio*, 2000; *Klahr and Bodenheimer*, 2006). In some of these models the vortices are simply prescribed and/or there is no feedback from the particles. Moreover, there are strong vertical velocities present in realistic vortices, and the vortical flows which concentrate m-sized particles are not found near the midplane, where the m-sized particles reside (*Barranco and Marcus*, 2005). Finally, there may be a tendency of particle concentrations formed in modeled vortices to drift out of them and/or destroy the vortex (*Johansen et al.*, 2004).

Another possibility of interest is the buildup of solids near the peaks of nearly axisymmetric, localized radial pressure maxima, which might for instance be associated with spiral density waves (*Haghighipour and Boss*, 2003a,b; *Rice et al.*, 2004). *Johansen et al.* (2006) noted boulder concentration in radial high pressure zones of their full simulation, but (in contrast to above suggestions about vortices), saw no concentration of meter-sized particles in the closest thing they could resolve in the nature of actual turbulent eddies. Perhaps this merely highlights the key difference between systematically rotating (and often artificially imposed) vortical fluid structures, and realistic eddies in realistic turbulence.

Overall, models of boulder concentration in large-scale fluid structures will need to assess the tendency for rapidly colliding meter-sized particles in such regions to destroy each other, in the real turbulence which will surely accompany such structures. For instance, breaking spiral density waves are themselves potent drivers for strong turbulence (*Boley et al.*, 2005).

3.4.2 Concentration of chondrules in 3D turbulence. Another suggestion for particle growth beyond a meter in turbulent nebulae is motivated by observed size-sorting in chondrites. *Cuzzi et al.* (1996, 2001) have advanced the model of turbulent concentration of chondrule-sized (mm or smaller diameter) particles into dense zones, that ultimately become the planetesimals we observe. This effect, which occurs in genuine, 3D turbulence (both in numerical models and laboratory experiments), naturally satisfies meteoritics observations in several ways under quite plausible nebula conditions. It offers the potential to leapfrog the problematic meter-size range entirely and would be applicable (to differing particle types) throughout the solar system (see *Cuzzi and Weidenschilling*, 2005 and *Cuzzi et al.*, 2005 for reviews). This scenario faces the obstacle that the dense, particle-rich zones which certainly *do* form are far from solid density, and might be disrupted by gas pressure or turbulence before they can form solid planetesimals. As

with dense midplane layers of small particles, gas pressure is a formidable barrier to gravitational instability on a dynamical timescale in dense zones of chondrule-sized particles formed by turbulent concentration. However, as with other small-particle scenarios, sedimentation is a possibility on longer timescales than that of dynamical collapse. It is promising that *Sekiya* (1983) found that zones of these densities, while “incompressible” on the dynamical timescale, form stable modes. Current studies are assessing whether the dense zones can survive perturbations long enough to evolve into planetesimals.

3.5. Summary of the situation regarding planetesimal formation

As of the writing of this chapter, the path to planetesimal formation remains unclear. In nonturbulent nebulae, a variety of options seem to exist for growth which - while not on dynamical collapse timescales, is rapid on cosmogonic timescales ($\ll 10^5$ years). However, this set of conditions and growth timescales seems to be at odds with asteroidal, meteoritic, and astronomical observations of several kinds (*Russell et al.*, 2006; *Dullemond and Dominik*, 2005; *Cuzzi and Weidenschilling*, 2006; *Cuzzi et al.*, 2005; chapter by *Wadhwa et al.*). The alternate set of scenarios - growth beyond a meter or so in size in turbulent nebulae - are perhaps more consistent with the observations but are still incompletely developed beyond some promising directions. The challenge is to describe quantitatively the rate at which planetesimals form under these inefficient conditions.

4. GLOBAL DISK MODELS WITH SETTLING AND AGGREGATION

Globally modeling a protoplanetary disk including dust settling, aggregation, radial drift and mixing, along with radiative transfer solutions for the disk temperature and spectrum form a major numerical challenge, because of the many orders of magnitude that have to be covered both in time scales (inner disk versus outer disk, growth of small particles versus growth of large objects) and particle sizes. Further numerical difficulties result from the fact that small particles may contribute significantly to the growth of larger bodies, and careful renormalization schemes are necessary to treat these processes correctly and in a mass-conserving manner (*Dullemond and Dominik*, 2005). Further difficulties arise from uncertainty about the strength and spatial extent of turbulence during the different evolutionary phases of a disk. A complete model covering an entire disk and the entire growth process along with all relevant disk physics is currently still out of reach. Work so far has therefore either focused on specific locations in the disk, or has used parametrized descriptions of turbulence with limited sets of physical growth processes. However, these “single slice” models have the problem that radial drift can become so large for m-sized objects, that these leave the slice on a time scale of a few orbital times (*Weidenschilling*, 1977; section 3.1.1). Nevertheless, important results have come

forth from these efforts, that test underlying assumptions of the models.

For the spectral and imaging appearance of disks, there are two main processes that should produce easily observable results: particle settling and particle growth. Particle settling is due to the vertical component of gravity acting in the disk on the pressure-less dust component (section 3.1.2). Neglecting growth for the moment, settling leads to a vertical stratification and size sorting in the disk. Small particles settle slowly and should be present in the disk atmosphere for a long time, while large particles settle faster and to smaller scale heights. While in a laminar nebula this is a purely time dependent phenomenon, this result is permanent in a turbulent nebula as each particle size is spread over its equilibrium scale height (*Dubrulle et al.*, 1995). From a pure settling model, one would therefore expect that *small dust grains* will increasingly dominate dust emission features (cause strong feature-to-continuum ratios) as large grains disappear from the surface layers.

Grain growth may have the opposite effect. While vertical mixing and settling still should lead to a size stratification, particle growth can become so efficient that all small particles are removed from the gas. In this case, dust emission features should be characteristic for *larger particles* (i.e. no or weak features, see chapter by *Natta et al.*). At the same time, the overall opacity decreases dramatically. This effect can become significant, as has been realized already early on (*Weidenschilling*, 1980, 1984; *Mizuno*, 1989). In order to keep the small particle abundance at realistic levels and the dust opacity high, *Mizuno et al.* (1988) considered a steady inflow of small particles into a disk. However, disks with signs of small particles are still observed around stars that seem to have completely removed their parental clouds, so this is not a general solution for this problem. In the following we discuss the different disk models documented in the literature. We begin with a discussion of earlier models focusing on specific regions of the solar system.

4.1. Models limited to specific regions in the solar system

Models considering dust settling and growth in a single vertical slice have a long tradition, and have been reviewed in previous Protostars and Planets III (*Cuzzi and Weidenschilling*, 1993). We therefore refrain from an in-depth coverage and only recall a few of the main results. The global models discussed later are basically similar calculations, with higher resolution, and for a large set of radii.

Weidenschilling has studied the aggregation in laminar (*Weidenschilling*, 1980, 2000) and turbulent (*Weidenschilling*, 1984, 1988) nebulae, focusing on the region of terrestrial planet formation, in particular around 1AU. These papers contain the basic descriptions of dust settling and growth under laminar and turbulent conditions. They show the occurrence of a rain-out after particles have grown to sizes where the settling motion starts to exceed the thermal motions. *Nakagawa et al.* (1981, 1986) study settling

and growth in vertical slices, also concentrating on the terrestrial planet formation regions. They find that within 3000 years, the midplane is populated by cm-sized grains. *Weidenschilling* (1997) studied the formation of comets in the outer solar system with a detailed model of a non-turbulent nebula, solving the coagulation equation around 30AU. In these calculations, growth initially proceeds by Brownian motion, without significant settling, for the first 10000yrs. Then, particles become large enough and start to settle, so that the concentration of solids increases quickly after $\times 10^4$ yr. The particle layer reaches the critical density where the layer gravitational instability is often assumed to occur, but first the high velocity dispersion prevents the collapse. Later, a transient density enhancement still occurs, but due to the small collisional cross section of the typically 1m-sized bodies, growth must still happen in individual 2-body collisions.

4.2. Dust aggregation during early disk evolution

Schmitt et al. (1997) implemented dust coagulation in an α disk model. They considered the growth of PCA in a one-dimensional disk model, i.e. without resolving the vertical structure of the disk. The evolution of the dust size distribution is followed for 100 years only. In this time, at a radius of 30AU from the star, first the smallest particles disappear within 10 years, due to Brownian motion aggregation. This is followed by a self-similar growth phase during which the volume of the particles increases by 6 orders of magnitude. Aggregation is faster in the inner disk, and the decrease in opacity followed by rapid cooling leads to a *thermal gap* in the disk around 3AU. Using the CCA particles, aggregation stops in this model after the small grains have been removed. For such particles, longer timescales are required to continue the growth.

Global models of dust aggregation during the prestellar collapse stage and into the early disk formation stage are numerically feasible because the growth of particles is limited. *Suttner et al.* (1999) and *Suttner and Yorke* (2001) study the evolution of dust particles in protostellar envelopes, during collapse, and the first 10 years of dynamical disk evolution, respectively. These very ambitious models include a radiation hydrodynamic code that can treat dust aggregation and shattering using an implicit numerical scheme. They find that during a collapse phase of 10 years, dust particles grow due to Brownian motion and differential radiative forces, and can be shattered by high velocity collisions cause by radiative forces. During early disk evolution, they find that at 30AU from the star within the first pressure scale height from the midplane, small particles are heavily depleted because the high densities lead to frequent collisions. The largest particles grow by a factor of 100 in mass. Similar results are found for PCA particles, while CCA particles show accelerated aggregation because of the enhanced cross section in massive particles. Within 10 years, most dust moves to the size grid limit of 0.2mm. While aggregation is significant near the midplane (opaci-

ties are reduced by more than a factor 10), the overall structure of the model is not yet affected strongly, because at the low densities far from the midplane aggregation is limited and changes in the opacity are only due to differential advection.

4.3. Global settling models

Settling of dust without growth goes much slower than settling that is accelerated by growth. However, even pure settling calculations show significant influence on the spectral energy distributions of disks. While the vertical optical depth is unaffected by settling alone, the height at which stellar light is intercepted by the disk surface changes. *Miyake and Nakagawa* (1995) computed the effects of dust settling on the global SED and compared these results with IRAS observations. They assume that after the initial settling and growth phase, enough small particles are left in the disk to provide an optically thick surface and follow the decrease of the height of this surface, concluding that this is consistent with the life-times of T Tauri disks, because the settling time of a 0.1 μm grain within a single pressure scale height is of order 10 Myr. However, the initial settling phase does lead to strong effects on the SED, because settling times at several pressure scale heights are much shorter.

Dullemond and Dominik (2004) show that settling from a fully mixed passive disk leads to a decrease of the surface height in 10^4 – 10^5 years, and can even lead to self-shadowed disks (see chapter by *Dullemond et al.*).

4.4. Global models of dust growth

Mizuno (1989) computes global models including evaporation, and a steady state assumption using small grains continuously raining down from the ISM. The vertical disk structure is not resolved, only a single zone in the midplane is considered. He finds that the Rosseland mean opacity decreases, but then stays steady due to the second generation grains.

Kornet et al. (2001) model the global gas and dust disk by assuming that at a given radius, the size distribution of dust particles (or planetesimals) is exactly monodisperse, avoiding the numerical complications of a full solution of the Smoluchowski equation. They find that the distribution of solids in the disk after 10^7 years depends strongly on the initial mass and angular momentum of the disk.

Ciesla and Cuzzi (2005) model the global disk using a four-component model: Dust grains, m-size boulders, planetesimals and the disk gas. This model tries to capture the main processes happening in a disk: growth of dust grains to m-sized bodies, the migration of m-sized bodies and the resulting creation of evaporation fronts, and the mixing of small particles and gas by turbulence. The paper focuses on the distribution of water in the disk, and the dust growth processes are handled by assuming timescales for the conversion from one size to the next. Such models are therefore mainly useful for the chemical evolution of the nebula and need detailed aggregation calculations as input.

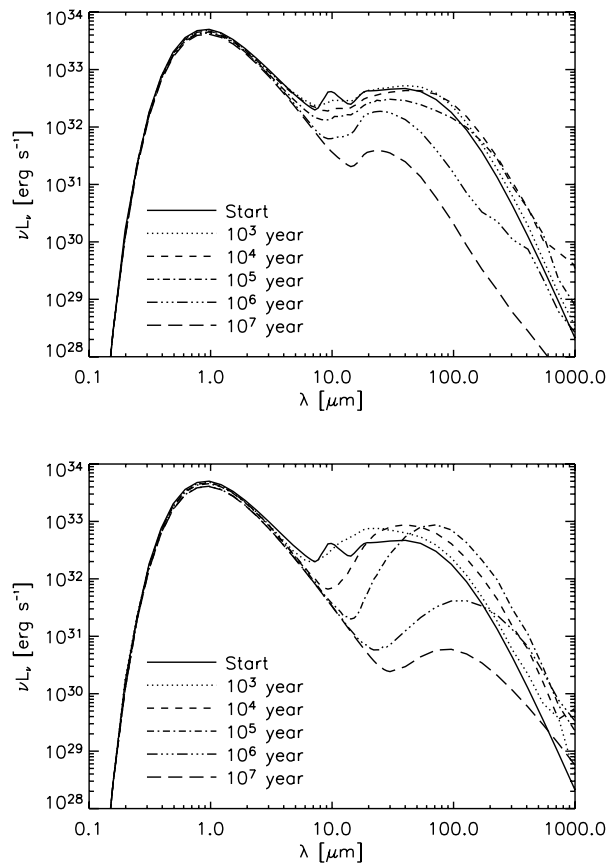


Fig. 5.— Time evolution of the disk SED in the laminar case (top panel) and the turbulent case (bottom panel). From DD05

The most complete long-term integrations of the equations for dust settling and growth are described in recent papers by *Tanaka et al.* (2005, henceforth TH105) and *Dullemond and Dominik* (2005, henceforth DD05). These papers implement dust settling and aggregation in individual vertical slices through a disk, and then use many slices to stitch together an entire disk model, with predictions for the resulting optical depth and SED from the developing disk. Both models have different limitations. TH105 consider only laminar disk models, so that turbulent mixing and collisions between particles driven by turbulence are not considered. Their calculations are limited to compact solid particles. DD05's model is incomplete in that it does not consider the contributions of radial drift and differential angular velocities between different particles. But in addition to calculations for a laminar nebula, they also introduce turbulent mixing and turbulent coagulation, as well as PCA and CCA properties for the resulting dust particles. TH105 use a two-layer approximation for the radiative transfer solution, while DD05 run a 3D Monte-Carlo radiative transfer code to compute the emerging spectrum of the disk. Both models find that aggregation proceeds more rapidly in the inner regions of the disk than in the outer regions, quickly leading to a region of low optical depth in the inner disk.

Both calculations find that a bi-modal size distribution is formed, with large particles in the midplane, formed by rainout (the fast settling of particles after their settling time has decreased below their growth time) and continuing to grow quickly, and smaller particles remaining higher up in the disk and then slowly trickling down. In the laminar disk, growth stops in the DD05 calculations at cm sizes because radial drift was ignored. In TH105, particles continue to grow beyond this regime.

The settling of dust causes the surface height of the disk to decrease, reducing the overall capacity of the disk to reprocess stellar radiation. TH105 find that at 8 AU from the star the optical depth of the disk at 10 μ m reaches about unity after a bit less than 10 yrs. In the inner disk, the surface height decreases to almost zero in less than 10 yrs. The SED of the model shows first a strong decrease at wavelength of 100 μ m and longer, within the first 10^5 yrs. After that the near-IR and mid-IR radiation also decreases sharply. TH105 consider their results to be roughly consistent with the observations of decreasing fluxes at near-IR and mm wavelengths in disks.

The calculations by DD05 show a more dramatic effect, as shown in Fig.5. In the calculations for a laminar disk, here the surface height already significantly decreases in the first 10 years, then the effect on the SED is initially strongest in the mid-IR region. After 10 yrs, the fluxes have dropped globally by at least a factor of 10, except for the mm regime, which is affected greatly only after a few times 10 years.

In the calculations for a turbulent disk (DD05), the depletion of small grains in the inner disk is strongly enhanced. This result is caused by several effects. First, turbulent mixing keeps the particles moving even after they have settled to the mid-plane, allowing them to be mixed up and rain down again through a cloud of particles. Furthermore, vertical mixing in the higher disk regions mixes low-density material down to higher densities, where aggregation can proceed much faster. The material being mixed back up above the disk is then largely deprived of solids, because the large dust particles decouple from the gas and stay behind, settling down to the mid plane. The changes to the SED caused by coagulation and settling in a turbulent disk are dramatic, and clearly inconsistent with the observations of disks around T Tauri stars that indicate lifetimes of up to 10^7 years. DD05 conclude that ongoing particle destruction must play an important role, leading to a steady-state size distribution for small particles (section 2.3.1).

4.5. The role of aggregate structure

Up to now, most solutions for the aggregation equation in disks are still based on the assumption of compact particles resulting from the growth process. However, at least for the small aggregates formed initially, this assumption is certainly false. First of all, if aggregates are fluffy, with large surface-to-mass ratios, it will be much easier to keep these particles in the disk surface where they can be ob-

served as scattering and IR emitting grains. Observations of the 10 μ m silicate features show that in many disks, the population emitting in this wavelength range is dominated by particles larger than interstellar (van Boekel *et al.*, 2005; Kessler-Silacci *et al.*, 2005). When modelled with compact grains, the typical size of such grains is several microns, with corresponding settling times less than a Myr. When modelled with aggregates, particles have to be much larger to produce similar signatures (flattened feature shapes, e.g. Min *et al.*, 2005).

When considering the growth time scales, in particular in regions where settling is driving the relative velocities, the timescales are surprisingly similar to the case of compact particles (Safronov, 1969, Weidenschilling, 1980). While initially, fluffy particles settle and grow slowly because of small settling velocities, the larger collisional cross section soon leads to fast collection of small particles, and fluffy particles reach the mid-plane as fast as compact grains, and with similar masses collected.

5. SUMMARY AND FUTURE PROSPECTS

A lot has been achieved in the last few years, and our understanding of dust growth has advanced significantly. There are a number of issues where we now have clear answers. However, a number of major controversies remain, and future work will be needed to address these before we can come to a global picture of how dust growth in protoplanetary disks proceeds and which of the possible ways toward planetesimals are actually used by nature. In table 1 on the following page we summarize our main conclusions and questions, and note some priorities for research in the near future.

Acknowledgments. We thank the referee (Stu Weidenschilling) for valuable comments on the manuscript. This work was partially supported by JNC's grant from the Planetary Geology and Geophysics program. CD thanks Kees Dullemond for many discussions, Dominik Paszun for preparing figure 1. JNC thanks Andrew Youdin for a useful conversation regarding slowly evolving, large scale structures.

REFERENCES

- Adachi I., Hayashi C., and Nakazawa K. (1976) *Prog. Theor. Phys.*, 56, 1756-1771.
- A'Hearn M. A. and the Deep Impact Team (2005) Deep Impact: The Experiment; 37th DPS, Cambridge, England, paper #35.02.
- Barge P., and Sommeria J. (1995) *Astron. Astrophys.*, 296, L1-L4.
- Barranco J. A. and Marcus P. S. (2005) *Astrophys. J.*, 623, 1157-1170.
- Bel N. and Schatzman E. (1958) *Rev. Mod. Phys.*, 30, 1015-1016.
- Blum J. (2004) in: *Astrophysics of Dust*, (A. Witt, G. Clayton and B. Draine, eds.), ASP Conference Series, Vol. 309, pp. 369-391.
- Blum J. (2006) *Advances in Physics*, submitted.
- Blum J. and Münch M. (1993) *Icarus*, 106, 151-167.

Table 1: Overview

What We Really Know	Main Controversies/Questions	Future Priorities
Microphysics		
<ul style="list-style-type: none"> – Dust particles stick in collisions with less than ~ 1 m/s velocity due to van der Waals force or hydrogen bonding. – For low relative velocities ($\ll 1$ m/s) a cloud of dust particles evolves into fractal aggregates ($D_f < 2$) with a quasi-monodisperse mass distribution. – Due to the increasing collision energy, growing fractal aggregates can no longer keep their structures so that non-fractal (but very porous) aggregates form (still at $v \ll 1$ m/s). – Macroscopic aggregates have porosities $> 65\%$ when collisional compaction, and not sintering or melting occurs. 	<ul style="list-style-type: none"> – At what aggregate size does compaction happen in a nebula environment? – When do collisions between macroscopic aggregates result in sticking? Some experiments show no sticking at rather low impact velocities, while others show sticking at high impact speeds. – How important are special material properties: organics, ices, magnetic and electrically charged particles? – What are the main physical parameters (e.g. velocity, impact angle, aggregate porosity/material/shape/mass) determining the outcome of a collision? 	<ul style="list-style-type: none"> – More empirical studies in collisions between macroscopic aggregates required. – Macroscopic model for aggregate collisions (continuum description) based on microscopic model and experimental results. – Develop recipes for using the microphysics in large scale aggregation calculations. – Develop aggregation models that treat aggregate structure as a <i>variable</i> in a self-consistent way.
Nebula processes		
<ul style="list-style-type: none"> – Particle velocities and relative velocities in turbulent and nonturbulent nebulae are understood; values are < 1 m/s for $a\rho < 1 - 3 \text{ g cm}^{-2}$ depending on alpha. – Radial drift decouples large amounts of solids from the gas and migrates it radially, changing nebula mass distribution and chemistry – Turbulent diffusion can offset inward drift for particles of cm size and smaller, relieving the “problem” about age differences between CAIs and chondrules. 	<ul style="list-style-type: none"> – What happens to dust aggregates in highly mass-loaded regions in the solar nebula, e.g. midplane, eddies, stagnation points? – Is the nebula turbulent? If so, how does the intensity vary with location and time? Can purely hydrodynamical processes produce self-sustaining turbulence in the terrestrial planet formation zone? – Can large-scale structures (vortices, spiral density waves) remain stable long enough to concentrate boulder-size particles? – Can dense turbulently concentrated zones of chondrule-size particles survive to become actual planetesimals? 	<ul style="list-style-type: none"> – Relative velocities in highly mass-loaded regions in the solar nebula, e.g. midplane, eddies, stagnation points. – Improve our understanding of turbulence production processes at very high nebula Reynolds numbers. – Model effects of MRI-active upper layers on dense, non-ionized gas in magnetically dead zones. – Model the evolution of dense strengthless clumps of particles in turbulent gas. – Model collisional processes in boulder-rich vortices and high-pressure zones. – Model evolution of dense clumps in turbulent gas.
Global modelling and comparison with observations		
<ul style="list-style-type: none"> – Small grains are quickly depleted by incorporation into larger grains. – Growth timescales are short for small compact and fractal grains alike. – Vertical mixing and small grain replenishment are necessary to keep the observed disk structures (thick/flaring). 	<ul style="list-style-type: none"> – What is the role of fragmentation for the small grain component? – Are the “small” grains seen really large, fluffy aggregates? – Are the mm/cm sized grains seen in observations compact particles, or much larger fractal aggregates? – What is the global role of radial transport? 	<ul style="list-style-type: none"> – Study the optical properties of <i>large</i> aggregates, fluffy and compact. – Implement realistic opacities in disk models to produce predictions and compare with observations. – Construct truly global models including radial transport. – More resolved disk images at many wavelengths, to better constrain models.

Blum J. and Schr apler R. (2004) *Phys. Rev. Lett.*, 93, 115503.

Blum J. and Wurm G. (2000) *Icarus*, 143, 138-146.

Blum J., Wurm G., Kempf S., Poppe T., Klahr H., *et al.* (2000) *Phys. Rev. Lett.*, 85, 2426-2429.

Blum J., Wurm G., Poppe T., and Heim L.-O. (1999) *Earth, Moon, and Planets*, 80, 285.

Bockel e-Morvan D., Gautier D., Hersant F., Hur e, J.-M., and Robert F. (2002), *Astron. Astrophys.*, 384, 1107-1118.

van Boekel R., Min M., Waters L. B. F. M., de Koter A., Dominik C., van den Ancker M. E., and Bouwman J. (2005), *Astron. Astrophys.*, 437, 189-208 .

Boley A. C., Durisen R. H., and Pickett M. K. (2005), *ASP Conf. Ser. 341: Chondrites and the Protoplanetary Disk*, 341,

839-848.

Bracco A., Provenzale A., Spiegel E. A., and Yecko P. (1998) in *Theory of Black Hole Accretion Disks* (M. A. Abramowicz, G. Bjornsson, and J. E. Pringle, eds.), pp. 254 Cambridge University Press.

Bridges F. G., Supulver K. D., and Lin D. N. C. (1996) *Icarus*, 123, 422-435.

Champney J. M., Dobrovolskis A. R., and Cuzzi J. N. (1995) *Physics of Fluids*, 7, 1703-1711.

Chandrasekhar S. (1961) *Hydrodynamic and Hydromagnetic Stability*, p. 589, Oxford University Press.

Chokshi A., Tielens A. G. G. M., and Hollenbach D. (1993) *Astrophys. J.*, 407, 806-819.

- Ciesla F. J. and Cuzzi J. N. (2005) *Icarus*, in press; also 36th LPSC CDROM.
- Colwell J. E. (2003) *Icarus*, 164, 188-196.
- Cuzzi J. N. (2004) *Icarus*, 168, 484-497.
- Cuzzi J. N. and Hogan R. C. (2003) *Icarus*, 164, 127-138.
- Cuzzi J. N. and Weidenschilling S. J. (2006) in *Meteorites and the Early Solar System II* (D. Lauretta, L. A. Leshin, and H. McSween, eds), Univ of Arizona Press; Tuscon, in press.
- Cuzzi J. N. and Zahnle K. (2004) *Astrophys. J.*, 614, 490-496.
- Cuzzi J. N., Ciesla F. J., Petaev M. I., Krot A. N., Scott E. R. D., and Weidenschilling S. J. (2005) *ASP Conf. Ser. 341: Chondrites and the Protoplanetary Disk*, 341, 732-773.
- Cuzzi J. N., Davis S. S., and Dobrovolskis A. R. (2003) *Icarus*, 166, 385-402.
- Cuzzi J. N., Dobrovolskis A.R., and Champney J. M. (1993) *Icarus*, 106, 102-134.
- Cuzzi J. N., Dobrovolskis A. R., and Hogan R. C. (1994) *Lunar Planet. Sci.*, XXV, 307-308, LPI, Houston.
- Cuzzi J. N., Dobrovolskis A. R., and Hogan R. C. (1996) in *Chondrules and the Protoplanetary Disk* (R. Hewins, R. Jones, and E. R. D. Scott, eds), pp. 35-44, Cambridge Univ. Press.
- Cuzzi J. N., Hogan R. C., Paque J. M., and Dobrovolskis A. R. (2001) *Astrophys. J.*, 546, 496-508.
- Cyr K., Sharp C. M., and Lunine J. I. (1999) *J. Geophys. Res.*, 104, 19003-19014.
- Dahneke B. E. (1975) *J. Colloid Interf. Sci.*, 1, 58-65.
- Davidsson B. J. R. (2006) *Advances in Geosciences*, in press.
- Derjaguin B. V., Muller V. M., and Toporov Y. P. (1975) *J. Colloid Interf. Sci.*, 53, 314-326.
- Desch S. J. and Cuzzi J. N. (2000) *Icarus*, 143, 87-105.
- Dobrovolskis A. R., Dacles-Mariani J. M., and Cuzzi J. N. (1999) *J.G.R. Planets*, 104, E12, 30805-30815.
- Dominik C. and Nübold H. (2002) *Icarus*, 157, 173-186.
- Dominik C. and Tielens A. G. G. M. (1995) *Phil. Mag.*, 72, 783-803.
- Dominik C. and Tielens A. G. G. M. (1996) *Phil. Mag.*, 73, 1279-1302.
- Dominik C. and Tielens A. G. G. M. (1997) *Astrophys. J.*, 480, 647-673.
- Dubrulle B., Morfill G. E., and Sterzik M. (1995) *Icarus*, 114, 237-246.
- Dullemond C. P. and Dominik C. (2004), *Astron. Astrophys.*, 421, 1075-1086.
- Dullemond C. P. and Dominik C. (2005), *Astron. Astrophys.*, 434, 971-986.
- Gail H.-P. (2004) *Astron. Astrophys.*, 413, 571-591.
- Garaud P. and Lin D. N. C. (2004) *Astrophys. J.*, 608, 1050-1075.
- Godon P. and Livio M. (2000) *Astrophys. J.*, 537, 396-404.
- Goldreich P. and Lynden-Bell D. (1965) *Mon. Not. R. Astron. Soc.*, 130, 97-124.
- Goldreich P. and Ward W. R. (1973) *Astrophys. J.*, 183, 1051-1061.
- Goodman J. and Pindor B. (2000) *Icarus*, 148, 537-549.
- Greenberg J. M., Mizutani H., and Yamamoto T. (1995) *Astron. Astrophys.*, 295, L35-L38.
- Gurevich L. E. and Lebedinsky A. I. (1950) *Izvestia Akademii Nauk USSR*, 14, 765.
- Gustafson B. Å. S. and Kolokolova L. (1999) *J. Geophys. Res.*, 104, 31711-31720.
- Haghighipour N. and Boss A. P. (2003a) *Astrophys. J.*, 583, 996-1003.
- Haghighipour N. and Boss A. P. (2003b) *Astrophys. J.*, 598, 1301-1311.
- Heim L., Blum J., Preuss M., and Butt H.-J. (1999) *Phys. Rev. Lett.*, 83, 3328-3331.
- Heim L., Butt H.-J., Schräpler R., and Blum J. (2005) *Aus. J. Chem.*, 58, 671-673.
- Henning T. and Stognienko R. (1996) *Astron. Astrophys.*, 311, 291-03
- Ivlev A. V., Morfill G. E., and Konopka U. (2002) *Phys. Rev. Lett.*, 89, 195502
- Jeans J. H. (1928) *Astronomy and Cosmogony*, Cambridge University Press, p. 337.
- Johansen A. and Klahr H. (2005) *Astrophys. J.*, 634, 1353-1371.
- Johansen A., Andersen A. C., and Brandenburg A. (2004) *Astron. Astrophys.*, 417, 361-374 .
- Johansen A., Klahr H., and Henning Th. (2006) *Astrophys. J.*, 636, 1121-1134.
- Karjalainen R. and Salo H. (2004) *Icarus*, 172, 328-348.
- Kempf S., Pfalzner S., and Henning Th. (1999) *Icarus*, 141, 388
- Kessler-Silacci J. E., Hillenbrand L. A., Blake G. A., and Meyer M. R. (2005), *Astrophys. J.*, 622, 404-429.
- Klahr H. and Bodenheimer P. (2006) *Astrophys. J.*, 639, 432-440.
- Konopka U., Mokler F., Ivlev A. V., Kretschmer M., Morfill, G.E., et al. (2005) *New Journal of Physics*, 7, 227, 1-11.
- Kornet K., Stepinski T. F., and Rózycka M. (2001) *Astron. Astrophys.*, 378, 180-191.
- Kouchi A., Kudo T., Nakano H., Arakawa M., Watanabe N., Sirono S.-I., Higa M., and Maeno N. (2002) *Astrophys. J.*, 566, L121-L124.
- Kozasa T., Blum J., and Mukai T. (1992) *Astron. Astrophys.*, 263, 423-432.
- Krause M. and Blum J. (2004) *Phys. Rev. Lett.*, 93, 021103.
- Krot A. N., Hutcheon I. D., Yurimoto H., Cuzzi J. N., McKeegan K. D., Scott E. R. D., Libourel G., Chaussidon M., Aleon J., and Petaev M. I. (2005) *Astrophys. J.*, 622, 1333-1342.
- Künzli S. and Benz W. (2003) *Meteoritics & Planetary Science*, 38, 5083.
- Love S. G. and Pettit D. R. (2004) *Lunar Planet. Sci.*, XXXV, Abstract #1119, LPI, Houston (CD-ROM).
- Markiewicz W. J., Mizuno H., and Völk H. J. (1991) *Astron. Astrophys.*, 242, 286-289.
- Marshall J. and Cuzzi J. (2001) *Lunar Planet. Sci.*, XXXII, 1262, LPI, Houston.
- Marshall J., Sauke T. A., and Cuzzi J. N. (2005) *Geophys. Res. Lett.*, 32, L11202-L11205.
- McCabe C., Duchêne G., and Ghez A. M. (2003) *Astrophys. J.*, 588, L113.
- Miyake K. and Nakagawa Y. (1995) *Astrophys. J.*, 441, 361-384.
- Mizuno H. (1989) *Icarus*, 80, 189-201.
- Mizuno H., Markiewicz W. J., and Voelk H. J. (1988) *Astron. Astrophys.*, 195, 183-192.
- Morfill G. E. and Völk H. J. (1984) *Astrophys. J.*, 287, 371-395.
- Nakagawa Y., Nakazawa K., and Hayashi C. (1981) *Icarus*, 45, 517-528.
- Nakagawa Y., Sekiya M., and Hayashi C. (1986) *Icarus*, 67, 375-390.
- Nübold H. and Glassmeier K.-H. (2000) *Icarus*, 144, 149-159.
- Nübold H., Poppe T., Rost M., Dominik C., and Glassmeier K.-H. (2003) *Icarus*, 165, 195-214.
- Nuth J. A. and Wilkinson G. M. (1995) *Icarus*, 117, 431-434.
- Nuth J. A., Faris J., Wasilewski P., and Berg O. (1994) *Icarus*, 107, 155-163.
- Ossenkopf V. (1993) *Astron. Astrophys.*, 280, 617-646.

- Paszun D. and Dominik C. (2006) *Icarus*, in press.
- Poppe T. and Schr apler R. (2005) *Astron. Astrophys.*, 438, 1-9.
- Poppe T., Blum J., and Henning Th. (2000a) *Astrophys. J.*, 533, 454-471.
- Poppe T., Blum J., and Henning Th. (2000b) *Astrophys. J.*, 533, 472-480.
- Rice W. K. M., Lodato G., Pringle J. E., Armitage P. J., and Bonnell I. A. (2004) *Mon. Not. R. Astron. Soc.*, 355, 543-552.
- Russell S. S., Hartmann L. A., Cuzzi J. N., Krot A. N., and Weidenschilling S. J. (2006) in *Meteorites and the Early Solar System, II* (D. Lauretta, L. A. Leshin, and H. McSween, eds.), in press.
- Safronov V. S. (1960) *Annales d'Astrophysique*, 23, 979-982.
- Safronov V. S. (1969) NASA TTF-677.
- Safronov V. S. (1991) *Icarus*, 94, 260-271.
- Salo H. (1992) *Nature*, 359, 619-621.
- Schmitt W., Henning Th., and Mucha R. (1997) *Astron. Astrophys.*, 325, 569-584.
- Scott E. R. D., Love S. G., and Krot A. N. (1996) in *Chondrules and the Protoplanetary Disk* (R. Hewins, R. Jones, and E. R. D. Scott, eds), pp. 87-96, Cambridge Univ. Press.
- Sekiya M. (1983) *Prog. Theor. Physics*, 69, 1116-1130.
- Sekiya M. (1998) *Icarus*, 133, 298-309.
- Sekiya M. and Takeda H. (2003) *Earth, Planets, and Space*, 55, 263-269.
- Sekiya M. and Takeda H. (2005) *Icarus*, 176, 220-223
- Shakura N. I., Sunyaev R. A., and Zilitinkevich S. S. (1978) *Astron. Astrophys.*, 62, 179-187.
- Sirono S. (2004) *Icarus*, 167, 431-452.
- Sirono S. and Greenberg J. M. (2000) *Icarus*, 145, 230-238.
- v. Smoluchowski M. (1916) *Physik. Zeit.*, 17, 557-585.
- Stepinski T. F. and Valageas P. (1996) *Astron. Astrophys.*, 309, 301-312.
- Stepinski T. F. and Valageas P. (1997) *Astron. Astrophys.*, 319, 1007-1019.
- Stone J. M., Gammie C. F., Balbus S. A., and Hawley J. F. (2000) in *Protostars and Planets IV* (V. Mannings, A. P. Boss, and S. S. Russell, eds.), pp. 589-599; Univ. of Arizona Press, Tucson.
- Supulver K. and Lin D. N. C. (2000) *Icarus*, 146, 525-540.
- Suttner G. and Yorke H. W. (2001) *Astrophys. J.*, 551, 461-477.
- Suttner G., Yorke H. W., and Lin D. N. C. (1999), *Astrophys. J.*, 524, 857-866.
- Tanaka H., Himeno Y., and Ida S. (2005), *Astrophys. J.*, 625, 414-426.
- Tanga P., Babiano A., Dubrulle B., and Provenzale A. (1996) *Icarus*, 121, 158-170.
- Tanga P., Weidenschilling S. J., Michel P., and Richardson D. C. (2004) *Astron. Astrophys.*, 427, 1105-1115.
- Toomre A. (1964) *Astrophys. J.*, 139, 1217-1238.
- T nyyi I., Guba P., Roth L. E., and Timko M. (2003) *Earth Moon and Planets*, 93, 65-74.
- Ueta T. and Meixner M. (2003) *Astrophys. J.*, 586, 1338-1355.
- V lk H. J., Jones F. C., Morfill G. E., and R ser S. (1980) *Astron. Astrophys.*, 85, 316-325.
- Valverde J. M., Quintanilla M. A. S., and Castellanos A. (2004) *Phys. Rev. Lett.*, 92, 258303
- Ward W. R. (1976) in *Frontiers of Astrophysics* (E. H. Avrett, ed.), pp. 1-40.
- Ward W. R. (2000) in *Origin of the Earth and Moon* (R. M. Canup et al., eds.), pp. 75-84, Univ. Arizona Press, Tucson.
- Wasson J. T., Trigo-Rodr guez J. M., and Rubin A. E. (2005) *Lunar Planet. Sci.*, XXXVI, Abstract #2314, LPI, Houston.
- Watson P. K., Mizes H., Castellanos A., and P rez A. (1997) in: *Powders & Grains 97*, (R. Behringer and J. T. Jenkins, eds), pp. 109-112, Balkema, Rotterdam.
- Weidenschilling S. J. (1977) *Mon. Not. R. Astron. Soc.*, 180, 57-70.
- Weidenschilling S. J. (1980) *Icarus*, 44, 172-189.
- Weidenschilling S. J. (1984), *Icarus*, 60, 553-567.
- Weidenschilling S. J. (1988) in *Meteorites and the early solar system* (J. A. Kerridge and M. S. Matthews, eds), pp. 348-371, University of Arizona Press, Tucson.
- Weidenschilling S. J. (1995) *Icarus*, 116, 433-435.
- Weidenschilling S. J. (1997) *Icarus*, 127, 290-306.
- Weidenschilling S. J. (2000) *Space Sci. Rev.*, 92, 295-310.
- Weidenschilling S. J. and Cuzzi J. N. (1993) *Protostars and Planets III*, 1031-1060.
- Whipple F. (1972) in *From Plasma to Planet* (A. Elvius, ed.), pp. 211-232, Wiley, New York.
- Wolf S. (2003) *Astrophys. J.*, 582, 859-868.
- Wurm G. and Blum J. (1998) *Icarus*, 132, 125-136.
- Wurm G. and Schnaiter M. (2002) *Astrophys. J.*, 567, 370-375.
- Wurm G., Blum J., and Colwell J. E. (2001) *Icarus*, 151, 318-321.
- Wurm G., Paraskov G., and Krauss O. (2004b) *Astrophys. J.*, 606, 983-987.
- Wurm G., Paraskov G., and Krauss O. (2005) *Icarus*, 178, 253-263.
- Wurm G., Relke H., Dorschner J., and Krauss O. (2004a) *J. Quant. Spect. Rad. Transf.*, 89, 371-384.
- Youdin A. N. (2004) *ASP Conf. Ser.*, 323, 319-327.
- Youdin A. N. and Chiang E. I. (2004) *Astrophys. J.*, 601, 1109-1119.
- Youdin A. and Shu F. (2002) *Astrophys. J.*, 580, 494-505.
- Yurimoto H. and Kuramoto N. (2004) *Science*, 305, 1763-1766.